Inorganic Chemistry

Article

pubs.acs.org/IC

Series of Uranyl-4,4′-biphenyldicarboxylates and an Occurrence of a Cation−Cation Interaction: Hydrothermal Synthesis and in Situ Raman Studies

Paula M. Cantos,[†] Laurent J. Jouffret,[‡] Richard E. Wilson,[§] Peter C. Burns,[‡] and Christopher L. Cahill*[,†]

[†]Department of Chemistry, The George Washington University, 725 21st Street NW, Washington, D.C. 20052, United States

[‡]Department of Civil and Environmental Engineering and Earth Sciences, University of Notre Dame, Notre Dame, Indiana 46556, United States

[§]Chemical Sciences and Engineering Division, Argonne National Laboratory, Argonne, Illinois 60439, United States

Supporting Information

ABSTRACT: Three uranium(VI)-bearing materials were synthesized hydrothermally using the organic ligand 4,4′-biphenyldicarboxylic acid: $(UO_2)(C_{14}O_4H_8)$ (**1**); $[(UO_2)_2(C_{14}O_4H_8)_2(OH)]\cdot(NH_4)(H_2O)$ (**2**); $(UO_2)_2(C_{14}O_4H_8)(OH)_2$ (**3**). Compound **1** was formed after 1 day at 180 °C in an acidic environment (pH_i = 4.03), and compounds **2** and **3** coformed after 3 days under basic conditions (pH_i = 7.95). Coformation of all three compounds was observed at higher pH_i (9.00). Ex situ Raman spectra of single crystals of **1**−**3** were collected and analyzed for signature peaks. In situ hydrothermal Raman data were also obtained and compared to the ex situ Raman spectra of the title compounds in an effort to acquire formation mechanism details. At pH_i = 4.00, the formation of **1** was suggested by in situ Raman spectra. At an increased pH_i (7.90), the in situ data implied the formation of compounds **1** and **3**. The most basic conditions (pH_i = 9.00) yielded a complex mixture of phases consistent with that of increased uranyl hydrolysis.

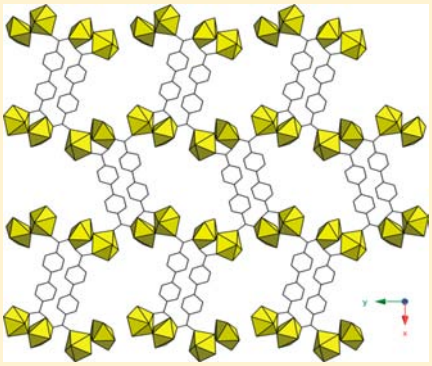

INTRODUCTION

Inorganic−organic hybrid materials, specifically coordination polymers, enjoy vast structural diversity because of the nearly limitless combinations of metals and organic ligands. Uranyl carboxylates are exemplary in this regard considering variation of the primary and secondary building units of uranium(VI) and thus provide a platform for a wide range of architectures.[1−9] These uranium-containing materials consist of uranyl metal centers linked through multitopic ligands to form extended topologies. This approach is typically employed by the more common d-block metal−organic framework materials (e.g., MOFs), which demonstrate an array of potential applications.[10−13] Actinide hybrid materials are admittedly more limited in their applications, yet understanding the fundamental actinide chemistry and relevance to the nuclear fuel cycle remains significant areas of inquiry, and hydrothermal syntheses thereof provide a forum for study in this area.

Uranium(VI)-bearing materials are typically constructed from the triatomic uranyl cation: a linear moiety composed of a central uranium atom capped with axial, terminal oxygen atoms.[14] In turn, the equatorial plane of $[UO_2]^{2+}$ contains accessible coordination sites, which give rise to three distinct primary building units of $[UO_2]^{2+}$: square, pentagonal, and hexagonal bipyramids.[14] Monomeric primary building units often oligomerize via hydrolysis to form secondary building units such as dimers, tetramers, chains, etc.[9,15,16] Coordination at the equatorial plane tends to promote, although not exclusively, one- and two-dimensional topologies observed in a majority of uranium(VI)-bearing hybrid compounds.[8]

Another interesting feature of uranyl hybrid materials is centered on the bonding of uranyl metal centers. Although the axial oxygen atoms of the uranyl cation are largely terminal, they have been observed as participants in cation−cation interactions (CCIs) with secondary metals, including other uranium(VI) centers.[17−20] In this scenario, the axial oxygen atom of one uranyl metal center is further coordinated to the equatorial position of a neighboring uranyl metal center. CCIs are more commonly displayed by the neptunyl cation, $[NpO_2]^+$, and a wide catalog of neptunium-containing CCIs has been reported. As such, a classification scheme of observed configurations of CCIs has been developed.[21,22] Recent studies of uranium(V), which is unstable in an aqueous solution because of disproportionation, have shown that CCIs are fairly common features for this oxidation state.[23]

An explanation of the occurrence of a uranium(VI)−uranium(VI) CCIs remains undeveloped, largely because of the fact that these interactions occur somewhat serendipitously, as does the one presented in this paper. Current research suggests the O═U═O bond can be weakened by either the coordination of electron-donating organic ligands or a basic coordination environment.[24−26] Solution-state chemistry has

Received: May 8, 2013
Published: August 2, 2013

   dx.doi.org/10.1021/ic401143g | *Inorg. Chem.* 2013, 52, 9487−9495

contributed to the understanding of CCIs in terms of their occurrence, formation mechanisms, and stability considerations.[20,27,28] Uranium(VI) CCIs are particularly intriguing because they are a departure from the traditional uranium(VI) equatorial binding configurations and may allow for the promotion of novel topologies.

The compounds described herein (and indeed the majority of uranyl coordination polymer materials) have been synthesized solvo(hydro)thermally and generally rely on ex situ methods, such as single-crystal X-ray diffraction, IR spectroscopy, and powder X-ray diffraction (PXRD), to accurately identify phases in bulk reaction products. Ex situ investigations on end products have allowed for systematic exploration of, for example, uranyl hydrolysis, as presented previously by our group.[15,29] End products may be significant in elucidating some formation details, yet a comprehensive understanding of reaction mechanisms is often lacking because of the inherent experimental challenges associated with probing hydrothermal syntheses. An in situ Raman investigation of hydrothermal systems, however, could prove beneficial in this regard. The coupling of ex and in situ Raman techniques could provide additional insight into the dynamic solution environment and formation mechanism details of hydrothermal uranyl systems when one considers the extensive literature surrounding both solid-state and solution-phase studies.[30−37]

In this contribution, we present the syntheses, crystal structures, fluorescence, and Raman spectroscopy of three uranium(VI) materials containing 4,4′-biphenyldicarboxyic acid (4,4′-BpDC; Figure 1): $(UO_2)(C_{14}O_4H_8)$ (**1**); $[(UO_2)_2(C_{14}O_4H_8)_2(OH)]\cdot(NH_4)(H_2O)$ (**2**); $(UO_2)_2(C_{14}O_4H_8)(OH)_2$ (**3**). It should be noted that **1** has been reported previously,[38] whereas **2** and **3** represent two new uranyl coordination polymers. Additionally, these compounds provide the opportunity to explore the spectroscopic Raman signatures of the uranyl cation and the influence of a uranium(VI) CCI. In this work, ex situ Raman spectra of the title uranyl-4,4′-BpDC materials were collected and used as a baseline to monitor the formation of **1**−**3** via hydrothermal in situ Raman spectroscopy. Moreover, with the introduction of a uranium(VI) CCI, we hope to contribute toward expanding the dialogue of actinide CCIs as a reproducible structural motif, as well as the spectroscopic signatures thereof.

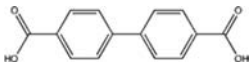

Figure 1. Structure of 4,4′-BpDC.

EXPERIMENTAL CONDITIONS

Synthesis. ***Caution!*** *While the uranyl nitrate hexahydrate, $UO_2(NO_3)_2\cdot 6H_2O$, used in these experiments contained depleted uranium, standard precautions for handling radioactive and toxic materials should be followed.*

All starting reagents in these syntheses are commercially available and used without any further purification. Compounds **1**−**3** were synthesized hydrothermally by preparing reaction mixtures of uranyl nitrate hexahydrate, 4,4′-BpDC, concentrated ammonium hydroxide, and distilled water (Table 1). The reactants were placed in a 23 mL Teflon-lined Parr reaction vessel and heated statically at 180 °C for 1 or 3 days. The reaction vessels were allowed to cool to room temperature over a period of 4 h, after which the mother liquor was decanted. The resulting crystals were washed with ethanol and distilled water and left to air-dry at room temperature. Compounds **2** and **3** coformed in the same reaction product in a ratio of 75:25, respectively (visual inspection). Despite attempts to achieve phase purity via modification of the synthetic conditions [see Table 1 in the Supporting Information (SI)], those reported in Table 1 remain the most reliable hydrothermal routes to producing both **2** and **3** in respectable yields and as quality single crystals. Moreover, Table 1 in the SI provides additional synthetic conditions that also yielded compounds **1**−**3**, as identified by PXRD.

Table 1. Synthetic Conditions for 1−3

	1	2	3
$UO_2(NO_3)_2\cdot 6H_2O$	0.103 g	0.100 g	0.100 g
4,4′-BpDC	0.097 g	0.096 g	0.096 g
NH_4OH	30 μL	60 μL	60 μL
H_2O	1.532 g	1.584 g	1.584 g
pH_i/pH_f	4.03/4.60	7.95/7.60	7.95/7.60
molar ratio	1:2:4.72:427	1:2:9.44:441	1:2:9.44:441
time (days)	1	3	3
crystal description	yellow plates	light-yellow hexagonal plates	dark-yellow hexagonal plates

Characterization. *Single-Crystal X-ray Structure Determination.* Single crystals from each of the bulk reaction products were isolated and mounted on MicroMount needle (MiTeGen). Reflections were collected from 0.5° φ and ω scans at 100 K on a Bruker SMART diffractometer equipped with an *APEX II* CCD detector and a Mo Kα source. The data were integrated with the *APEX II* software suite[39] and corrected for absorption using *SADABS*.[40] The structures of compounds **2** and **3** were solved using direct methods and refined using *SHELX-97*[41] within the *WinGX*[42] software suite. Selected crystallographic data are provided in Table 2. All non-hydrogen atoms were located in difference Fourier maps and ultimately refined anisotropically. Hydrogen atoms residing on parent carbon atoms of 4,4′-BpDC were placed in calculated positions for **2** and **3**. The hydrogen atoms on solvent water molecules and ammonium cations in **2** were located in the difference Fourier map but could not be successfully modeled or refined. The positional disorder of 4,4′-BpDC in **2** was modeled appropriately. Bound hydroxyl groups on uranyl centers in **2** and **3** were identified using bond-valence summations (Tables 2 and 3 in the SI).

Table 2. Crystallographic Data and Structure Refinement for 2 and 3

	2	3
empirical formula	$C_{28}H_{16}NO_{14}U_2$	$C_{14}H_8O_{10}U_2$
fw	1066.48	826.27
temperature (K)	100	100
cryst syst	monoclinic	monoclinic
space group	$C2/c$	$P2_1/c$
a (Å)	31.061(9)	16.6217(6)
b (Å)	15.409(4)	10.2529(3)
c (Å)	13.956(4)	10.4232(3)
α (deg)	90	90
β (deg)	115.612(4)	101.1000(10)
γ (deg)	90	90
V (Å^3)	6024(3)	1743.10(10)
Z	2	4
D_{calc} (g cm^{-3})	2.352	3.149
μ (mm^{-1})	10.813	18.613
R_{int}	0.0739	0.0684
R1[a] [$I > 2\sigma(I)$]	0.0363	0.0323
wR2[a]	0.0828	0.0754

[a] $R1 = \sum||F_o| - |F_c||/\sum|F_o|$; $wR2 = \{\sum w(F_o^2 - F_c^2)^2/\sum w(F_o^2)^2\}^{1/2}$.

dx.doi.org/10.1021/ic401143g | Inorg. Chem. 2013, 52, 9487−9495

PXRD. PXRD data of bulk reaction products were collected using a Rigaku Miniflex (Cu Kα, 2θ = 3–60°) and manipulated using the *JADE* software package.[43] The PXRD data of the ex situ hydrothermal syntheses are provided in Figures 1–3 in the SI. At an acidic pH (4.03), compound **1** and a uranyl oxide hydrate (PDF 16-0207) are the only discernible phases within the bulk reaction product, while at more basic pH ranges (7.95 and 9.00), however, the PXRD data display a mixture of compounds **1**–**3** highlighting the complexity of end products as a consequence of uranyl hydrolysis.

Single-Crystal Fluorescence. Fluorescence data were acquired on all compounds from single crystals using a Craic Technologies UV–vis–near-IR microspectrophotometer with a fluorescence attachment. Excitation was achieved using 365 nm light from a mercury lamp. Emission spectra for compounds **1**–**3** are provided in Figure 7 in the SI.

RESULTS

Structural Description. Compound **1**, $(UO_2)(C_{14}O_4H_8)$, was reported previously,[38] yet for context, a brief description follows. The structure is composed of one crystallographically unique uranyl metal center adopting square-bipyramidal geometry, as seen in Figure 2. These square bipyramids are

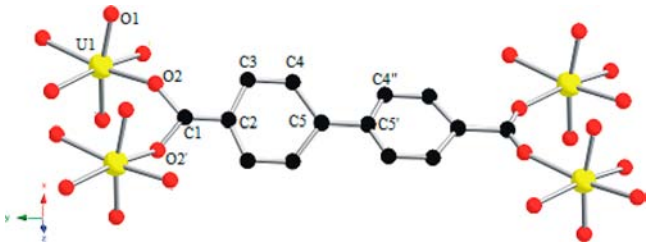

Figure 2. Ball-and-stick representation of **1**. The yellow spheres represent uranium metal centers, red spheres represent oxygen atoms, and black spheres represent carbon atoms.

then linked via bridging bidentate 4,4′-BpDC linkers to form two-dimensional sheets. The axial and equatorial bond distances of **1** are representative of typical of uranium(VI)-bearing materials and are provided in Table 3. Figure 2 also highlights the rotational ability of the 4,4′-BpDC ligand, as evidenced by a torsion angle of 26.35° between carbon atoms C4, C5, C5′, and C4″. The extended sheet topology of **1** can be seen in Figure 3.

The crystal structure of **2**, $[(UO_2)_2(C_{14}O_4H_8)_2(OH)]\cdot(NH_4)(H_2O)$, also displays a two-

Table 3. Selected Bond Lengths (Å) of 2 and 3

2		3	
U1–O1	1.769(4)	U1–O1	1.820(4)
U1–O2	1.769(4)	U1–O2	1.785(4)
U1–O3	2.296(4)	U1–O3	2.390(4)
U1–O4	2.472(4)	U1–O4	2.237(4)
U1–O5	2.463(4)	U1–O5	2.340(4)
U1–O6	2.349(4)	U1–O6	2.458(4)
U1–O7	2.349(4)	U1–O7	2.326(4)
U2–O8	1.775(4)	U2–O8	1.782(4)
U2–O9	1.776(4)	U2–O9	1.794(4)
U2–O6	2.306(4)	U2–O3	2.333(5)
U2–O10	2.320(4)	U2–O4	2.262(4)
U2–O11	2.360(4)	U2–O10	2.455(4)
U2–O12	2.471(4)	U2–O11	2.360(4)
U2–O13	2.320(4)	U2–O1	2.480(4)

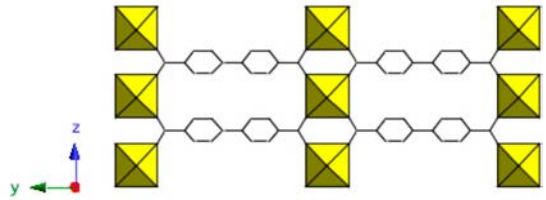

Figure 3. Polyhedral representation of a single sheet within **1**. Yellow polyhedra represent uranium metal centers, and black lines represent C–C bonds.

dimensional topology, yet uranium metal centers are in a pentagonal-bipyramidal geometry and exist as point-shared dimers. Figure 4 highlights the local structure of **2**: two point-

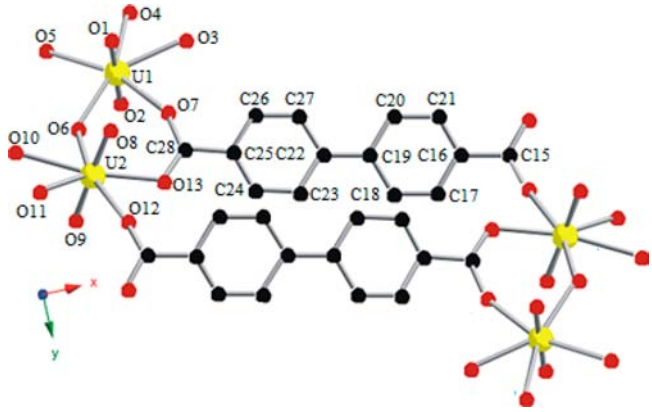

Figure 4. Ball-and-stick representation of the local structure of **2**.

sharing, crystallographically independent uranyl cations, U1 and U2, coordinated in a bridging bidentate manner to 4,4′-BpDC through carboxylate oxygen atoms O7 and O13. Selected axial and equatorial U–O bonds are compiled in Table 3. Bond-valence summations for **2** (Table 3 in the SI) indicate a hydroxide ion at O6.[44,45] The anionic sheets form pseudo-channels when stacked (Figure 5) in which water and ammonium molecules reside, the latter of which provides charge balance.

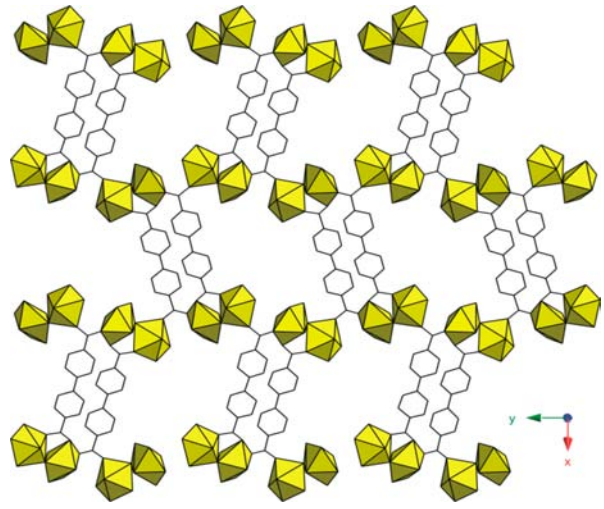

Figure 5. Polyhedral representation of the two-dimensional sheets of **2**. Interlayer ammonium and water molecules were omitted for clarity.

dx.doi.org/10.1021/ic401143g | *Inorg. Chem.* 2013, 52, 9487–9495

Compound **3**, $(UO_2)_2(C_{14}O_4H_8)(OH)_2$, is also composed of point-sharing uranyl pentagonal bipyramids. Similar to **2**, neighboring uranyl cations are bound via bridging bidentate carboxylate groups of 4,4′-BpDC, as seen in Figure 6. The bond valence confirms O4 and O5 as hydroxides within compound **3**.

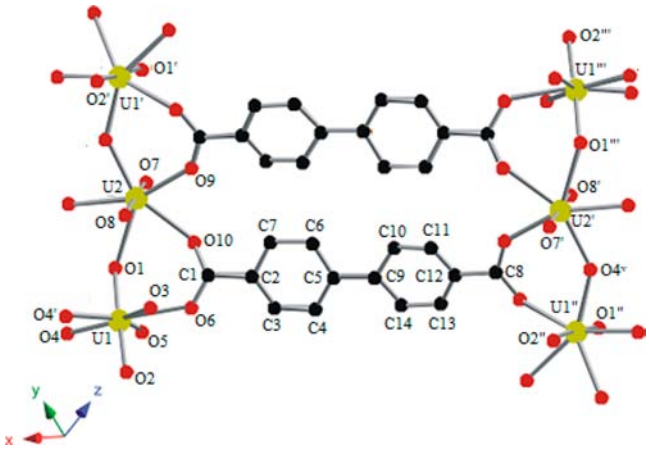

Figure 6. Ball-and-stick representation of the local structure of **3**.

U1 and U2 are two crystallographically unique metal centers, which are point-sharing and edge-sharing, as illustrated in Figure 7. An overall three-dimensional architecture is

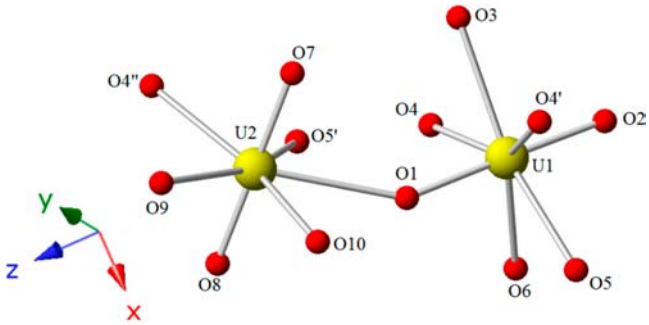

Figure 7. Ball-and-stick representation of the CCI in **3**.

propagated through the coordination of 4,4′-BpDC and oligomerized uranium atoms. The ball-and-stick model of **3** (Figure 7) highlights the CCI between U1 and U2. Oxygen atom O1 caps one end of O═U1═O and is also one of five equatorial oxygen atoms coordinated to U2. As a consequence of the CCI, the U1−O1 axial bond is elongated to a distance of 1.820(4) Å compared to the U1−O2 axial length [1.785(4) Å]. Similarly, the equatorial U2−O1 bond length is longer [2.480(4) Å] than its neighboring equatorial bonds in **3** (Table 3).

DISCUSSION

Structural Description. Three uranyl-4,4′-BpDC materials were synthesized by modifying the pH and time, allowing us to monitor the influence of uranyl hydrolysis on product formation. Variation of the synthetic conditions exposed a complex system of reaction products, especially at higher pH values, as seen in Table 1 in the SI. These compounds provided a basis for comparing and contrasting structural topologies as well as spectroscopic attributes.

The landscape of reported uranium hybrid materials is indeed dominated by two-dimensional structures, as is the case of **1**. The structure of this material (Figure 3) displays bidentate coordination of 4,4′-BpDC to monomeric units of square-bipyramidal uranium atoms, which form two-dimensional sheets. Similar to **1**, compound **2** is also composed of sheets, yet dimers of point-shared pentagonal bipyramids replace the monomeric square-bipyramidal geometry of $[UO_2]^{2+}$ observed in **1** (Figure 4). As shown in Table 1, **2** was synthesized in a basic environment (pH_i = 7.95), increasing the likelihood of promoting polynuclear secondary building units.

Compounds **2** and **3** coform in the same bulk reaction product, yet their pentagonal bipyramids display two different forms of oligomerization: point- and edge-sharing. Because syntheses of these compounds occurred at a higher pH (7.95), this result is consistent with the premise of uranyl hydrolysis. Perhaps most intriguing, however, is the presence of a CCI observed in **3**, as shown in Figure 7.

In the most general terms, a CCI can be defined as the direct coordination between two distinct metal centers. Compound **3** contains a uranyl−uranyl CCI, as illustrated in Figure 7, where oxygen atom O1 is axial to U1, while simultaneously participating in an equatorial U−O bond with U2. Actinyl−actinyl CCIs are more commonly observed between neptunyl cations, $[NpO_2]^+$, and have been examined thoroughly by Krot and Grigoriev,[21] who developed a detailed classification system of CCI geometries. Of the eight types of CCIs they have delineated, compound **3** is denoted as having "type a" interactions.[21]

Solution-state chemistry has provided the earliest example of an actinide CCI, as well as the origin of the CCI designation.[20] Since then, complexes in both the solution and solid state have peppered the literature and mainly focus on CCIs of $[AnO_2]^+$ compounds.[27,28,46−48] This growing catalog has provided a basis for spectroscopic studies and a further developed rationalization of the occurrence of CCIs in $[AnO_2]^+$-containing materials.[27,28] Recently, Loiseau et al. and zur Loye et al. have published results contributing to the catalog of uranium(VI)−uranium(VI) CCI materials.[17,48,49] The presence of uranium(VI) CCIs in the literature has been sporadic, arguably because of gaps in our understanding of the formation requirements for solid-state compounds. This challenge can be addressed by developing a synthetic method for promoting the production of uranium(VI) CCIs as a desired topological feature. At present, careful structural analysis of CCI occurrences may contribute to this effort.

Raman Studies. *Single-Crystal ex Situ Raman Spectroscopy.* Raman spectra were collected from randomly oriented single crystals using a Renishaw inVia Raman microscope employing a 785 nm excitation source (circularly polarized) and 1200 mm^{-1} grating. The crystals were placed on a standard microscope slide containing a concave well and covered with a standard glass coverslip. Each spectrum represents the average of 100 1-s exposures. Energy calibrations were performed using the Raman scattering line of an internal silicon reference.

Figure 8 displays the vibrational modes of the $[UO_2]^{2+}$ cation of interest in this study: a Raman-allowed (IR-forbidden) symmetric stretch (ν_1) and an IR-allowed (Raman-forbidden) asymmetric stretch (ν_3). In the complexes reported here, molecule site group analysis of the uranyl ions demonstrates that the symmetric and asymmetric vibrational modes of the uranyl unit are relaxed, a consequence of the reduced symmetry of these ions in the solid state.

dx.doi.org/10.1021/ic401143g | Inorg. Chem. 2013, 52, 9487−9495

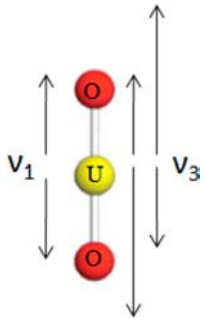

Figure 8. Ball-and-stick representation of the uranyl cation, $[UO_2]^{2+}$. The vibrational frequencies ν_1 and ν_3 are $[UO_2]^{2+}$ symmetric and antisymmetric stretches, respectively.

The reduced site symmetry of U1 in **1** (C_2) results in the relaxation of the selection rules, making the symmetric and asymmetric modes both Raman- and IR-active. The symmetric stretch (ν_1) is represented in the Raman spectrum at 848 cm^{-1} and its corresponding IR stretch (ν_3) at 932 cm^{-1}. The sharp band in the IR spectrum imposed on the ν_1 mode in the Raman spectrum is assigned to the bending modes of the aromatic C−H′s of 4,4′-BpDC and not the ν_3 mode of uranyl, which would be expected to be much weaker in intensity despite relaxation of the selection rules. Two minor Raman peaks in compound **1** (~750 and 800 cm^{-1}) are also assigned to the vibrational ligand modes (Figure 9a). It is important to note that peak intensities can be influenced by single-crystal orientation during data collection and may be the reason for more intense C−H peaks in **2** and **3** (Figure 9b,c).

The Raman and IR spectra for **2** and **3** are more complex. The Raman spectrum for **2** (Figure 9b) displays a strong peak at 873 cm^{-1}; however, this feature is tentatively assigned as the symmetric stretch. Definitive assignments of the bands in this spectrum are complicated by the significant interference from vibrational modes attributable to the ligand. The split peaks between 810 and 850 cm^{-1} in both Raman and IR spectra are generated from the C−H bonds in the aromatic rings of 4,4′-BpDC.

Compound **3** exhibits unique coordination environments of U1 and U2, which produce two distinct peaks observed in the Raman spectrum (Figure 9c) as well as peaks in the IR spectrum. This oligomer is also of particular interest from a spectroscopic perspective considering the presence of a uranium(VI) CCI. The increased U═O bond length of U1 increasing the asymmetry in the U═O bond may correspond to the lower frequency peak at 829 cm^{-1}. The symmetric U═O bonds in U2 have a corresponding Raman peak at 855 cm^{-1}, whereas the peaks lower than 800 cm^{-1} are characteristic of the C−H bonds from 4,4′-BpDC. This relationship between decreasing U═O symmetry and Raman frequency has recently been explored by Loiseau et al.[49] These authors have observed that an elongated axial U═O bond distance due to a uranium(VI) CCI, when compared to other axial U═O bond distances of the neighboring uranium metal centers, generated a Raman peak with a decreased frequency of 810 cm^{-1}. The peak assignments for single crystals of compounds **1**−**3** are consistent with those in previous uranyl Raman investigations.[50−52] In addition, assignments from crystallographic parameters using the Bartlett equation were attempted.[53] This approach yielded mixed results yet may be found in the SI.

In Situ Raman Spectroscopy. The synthesis results of our uranyl(VI)-4,4′-BpDC system presented a complex scheme of reaction products, as indicated by Table 1 in the SI. Specific combinations of pH and time yielded single crystals of the title compounds, yet the complexity of the coformation of **1**−**3**, especially between pH values of 5 and 11, inhibits ex situ investigations regarding formation mechanisms. Also, the nature of hydrothermal syntheses (e.g., steel reaction vessels) precludes a comprehensive investigation of other phases forming during the reactions. To explore this hydrothermal environment, we employed in situ Raman spectroscopy to observe the dynamic aqueous environment and acquire a greater understanding of the formation of compounds **1**−**3**. By combining the results of ex and in situ Raman data, we can ideally monitor the mechanism and speciation of uranium solid-state products in the reaction solution. As such, ex situ Raman data were collected on single crystals of the title compounds

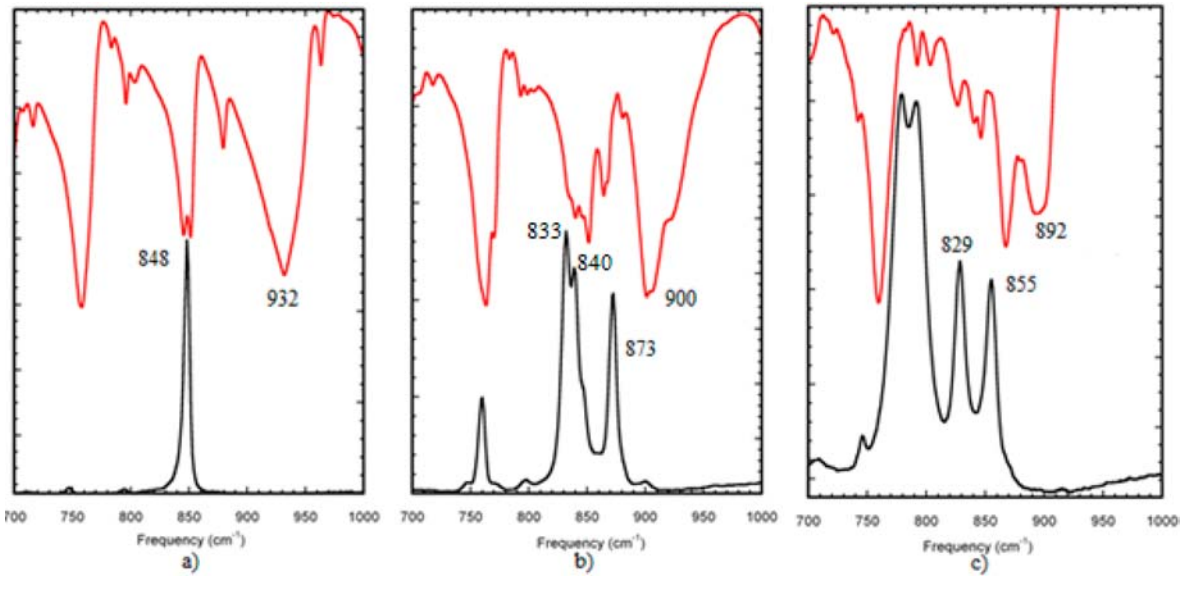

Figure 9. Raman and IR spectra of (a) **1**, (b) **2**, and (c) **3**. Black lines (bottom) represent Raman spectra, and red lines (top) represent IR spectra.

dx.doi.org/10.1021/ic401143g | Inorg. Chem. 2013, 52, 9487−9495

and then compared to Raman data produced by the hydrothermal in situ apparatus.

The setup of the in situ Raman spectroscopy experiment has been described in detail earlier, yet Figure 10 provides a schematic of the instrument.[54]

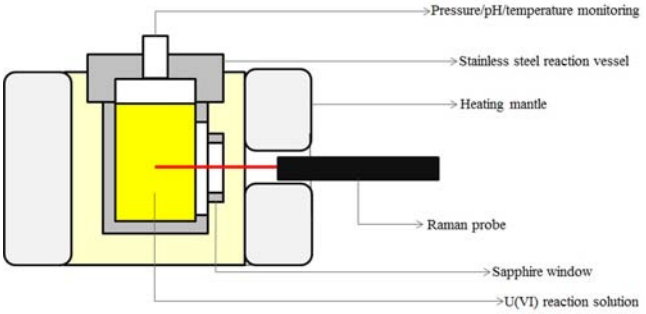

Figure 10. Schematic of the hydrothermal in situ Raman apparatus.

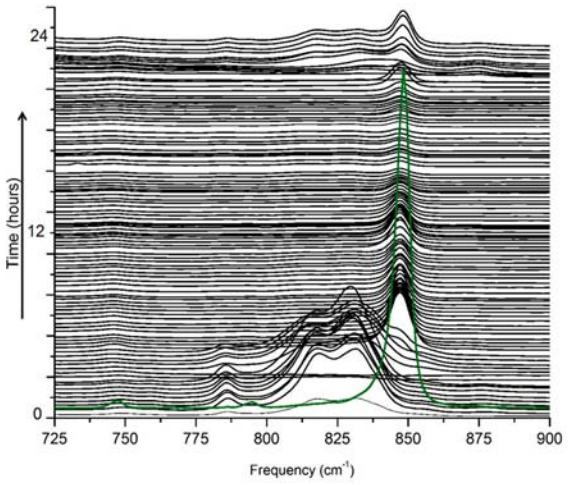

Figure 11. Portion of the in situ Raman spectra obtained at 180 °C after 1 day at pH_i = 4.00. The ex situ Raman of **1** is represented by the solid green line.

The Raman spectra were collected from solutions using a Bruker Sentinel system linked via fiber optics to a video-assisted Raman probe equipped with a 785 nm, 400 mW laser and a high-sensitivity, TE-cooled, 1024 × 255 CCD array. The spectra were collected for 60 s with 10 signal accumulations, in the range from 80 to 3200 cm^{-1}. The Parr vessel (100 mL) was loaded with 1000 mg of $UO_2(NO_3)_2{\cdot}6H_2O$ and 960.0 mg of 4,4′-BpDC. The reaction mixture was created by adding 30 mL of deionized water and agitating the vessel to get the solid reagents into solution. The pH was adjusted to 4.00, 7.90, and 9.00 with concentrated NH_4OH.

Each mixture at the corresponding pH was heated from room temperature to 70 °C over 30 min, from 70 to 80 °C over 30 min, followed by soaking at 80 °C for 30 min, and heating to 90 °C over 30 min. This heating/holding pattern was continued until the temperature reached 180 °C. After reaching 180 °C, the reactor was held at temperature for the required number of days and was then cooled to 70 °C according to the reverse of the protocol used for heating, at which point the heating mantle was turned off. Spectra were recorded every 1800 s beginning with the heating program, and background measurements were systematically recorded before each spectrum.

pH = 4.00 Spectra. As shown in Figure 11, a signal consistent with compound **1** (green) is observed in the in situ Raman spectra (black lines). The signal of **1** (848 cm^{-1}) appears 7.5 h into the reaction process and stabilizes at 180 °C as the remaining product in the reaction solution, which indicates a monodisperse uranyl speciation profile consistent with low-pH conditions.

Prior to the formation and stabilization of **1**, however, are broad features from 815 to 830 cm^{-1} as well as a peak located at 785 cm^{-1}. These are likely the result of a range of hydrolysis products present in solution prior to the emergence and crystallization of **1**. As the reaction progressed, these phases were consumed within the reaction solution (around 4.5 h), as indicated by the disappearance of their corresponding signals, after which the appearance of the peak at 848 cm^{-1} was observed. This is suggestive of the initial mixture of phases ultimately developing into a single-component system. These peak assignments are consistent with a previous Raman study of uranyl hydrolysis products by Toth and Begun,[55] wherein the formation of three distinct monomeric, dimeric, and trimeric uranyl complexes over a pH range at 1.3−4.02 was investigated.

pH = 7.90 Spectra. In situ studies at a higher pH range were of key interest because of the coformation of compounds **2** and **3** (Table 1 in the SI) under these conditions. By utilizing a similar pH value in our in situ Raman exploration, it was hoped that we would acquire details of the formation mechanism(s) of **2** and **3**. Parts a−c of Figure 12 show segments of in situ Raman spectra collected over a period of 3 days covering three different temperature regions at pH_i = 7.90. Upon heating to 180 °C (day 1, Figure 12a), the in situ Raman spectra display peaks between the range of 750−875 cm^{-1}, with peaks at 750, 785, and 860 cm^{-1} representing unidentified, minor phases, yet are likely consistent with those we have described for the pH = 4.00 studies. The peak around 848 cm^{-1} appears early in the data collection and was identified as compound **1**. As day 1 progressed, a signal at 825 cm^{-1} appeared in the spectra and remained into day 2 when the reaction vessel was stabilized at 180 °C. This peak may be tentatively assigned to compound **3**, although the absence of a signal at 855 cm^{-1} adds uncertainty to this identification (Figure 12b). That said, definitive comparisons between in situ and ex situ data for these compounds should be made with caution because it appears that, as the number of unique uranyl sites in a structure increases, our ability to explicitly identify phases diminishes.

Figure 12c displays the cooling stage from 180 °C to room temperature of the reaction solution. Again, a peak at 848 cm^{-1} was present in the in situ spectra and corresponds to compound **1**. The spectra obtained at pH_i = 7.90 suggest that only compounds **1** and **3** could be identified and remain as our best interpretation of the Raman data. The complexity of the spectra, especially those collected during day 2, required a closer examination in order to identify phases. Parts a−c of Figure 8 in the SI display the spectra from day 2 overlaid with the ex situ spectra of each of the title compounds. From this, we concluded that the ex situ spectra of compound **3** (Figure 8b in the SI) produced the best match to the in situ spectra of day 2 at pH = 7.90. At higher pH ranges, it is also important to acknowledge decreasing "free" uranyl concentration within the reaction solution because of the precipitation of oligomeric phases, which may explain the disappearance of **3** throughout

dx.doi.org/10.1021/ic401143g | Inorg. Chem. 2013, 52, 9487−9495

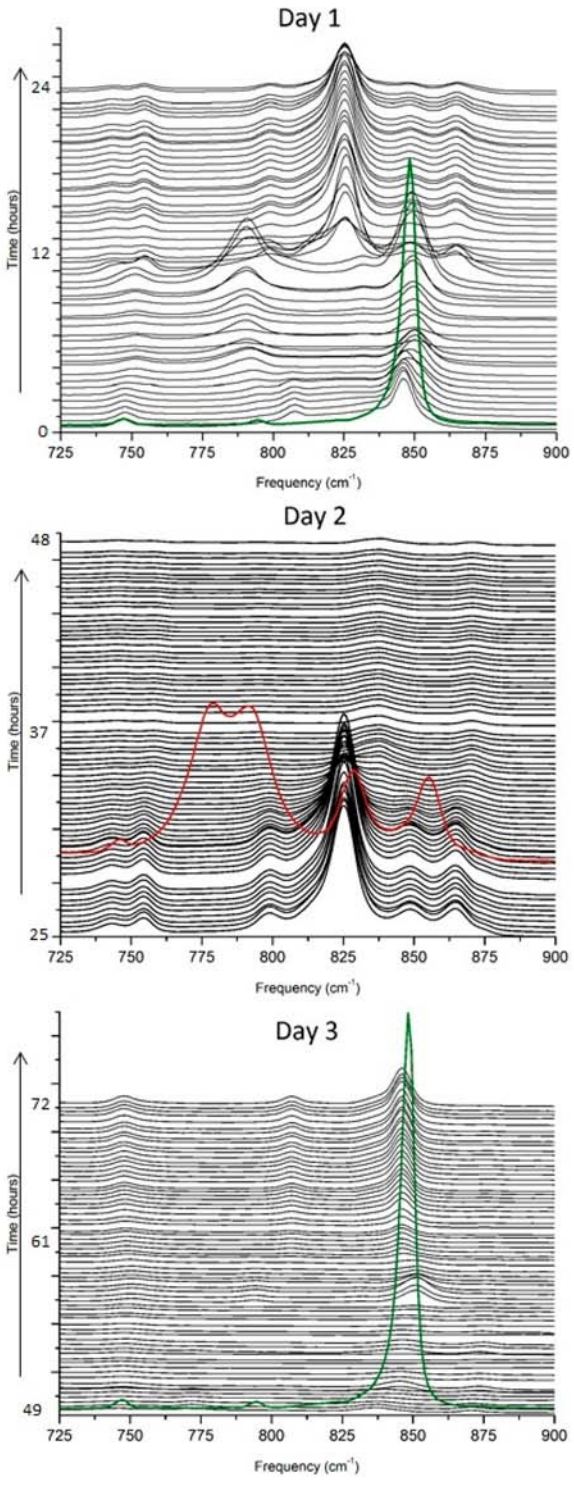

Figure 12. In situ Raman spectra at pH = 7.90 at (a) day 1 (heating from room temperature to 180 °C; the solid green line represents the ex situ Raman spectrum of **1**); (b) day 2 (stabilization at 180 °C; the solid red line represents the ex situ Raman spectrum of **3**); (c) day 3 (cooling from 180 °C to room temperature; again, the solid green line represents the ex situ Raman spectrum of **1**).

day 2 and the distinct manifestation of a monomeric compound (**1**) within the solution at the end of day 3.

pH = 9.00 Spectra. All three compounds had been observed to form at this pH condition (Table 1 in the SI); therefore, it was of interest to explore the formation order. If one considers uranyl hydrolysis, as the pH increases, so does the variation and complexity of uranyl species within a reaction solution.[15,56] Thus, a diverse suite of uranyl species in both the solid state and solution phase is present, making it difficult to deconvolve in situ Raman spectra. Parts a–c of Figure 9 in the SI represent the in situ Raman spectra collected over a period of 3 days. We can conclude that the reaction solution presents a complicated mixture of uranyl species, making it difficult to detect and confirm the presence of compounds **1**–**3**. We, therefore, offer these data strictly for informational purposes and make no attempt to extract formation mechanism details.

In general, one should comment on the signal shifts observed within not only these in situ Raman data but also previously reported solution-phase Raman studies.[33,56–59] For compounds **1**–**3**, a comparison of ex and in situ Raman spectra revealed shifts between the observed peaks. At this point, it is still difficult to specify the underlying cause for this occurrence, yet previous studies indicate that the surrounding environment of the uranyl cation is a key contributor.[60,61] Nguyen-Trung et al. investigated aqueous uranyl complexes under acidic and basic conditions and demonstrated that an increase of coordinated hydroxide ions consequently decreased the observed vibrational frequency of the uranyl complex.[60] One may therefore argue that the variance between ex and in situ Raman signals stems from the differences between static and well-defined uranyl coordination within solid-state structures versus the dynamic and complex coordination in the solution phase. Moreover, disparities between ex and in situ generated Raman data may also be addressed by differences in the experimental parameters. The end products from hydrothermal (ex situ) data were synthesized in a sealed Teflon liner, while the hydrothermal in situ Raman studies used a glass liner. Additionally, the larger volume of the in situ reaction (with less effective sealing) required a proportional increase of all starting reagents, thus affecting the internal pressure and potentially speciation. It is also possible that aggregation of solid product on the sapphire window (Figure 10) may occur and generate Raman spectra of solid as well as solution phases. The design of the heating mantle induces a convection current within the solution reaction mixture, yet it is difficult to determine its influence on product aggregation. Perhaps future modifications, which include a built-in agitator, may limit the amount of crystallization obscuring the sampling window, if, in fact, present. While the results reported herein are indeed informative and speak to the complexity of uranyl hydrolysis under hydrothermal conditions,[29] we caution against an "overinterpretation" of the in situ spectra and thus offer these observations in a more qualitative manner.

PXRD. *End Products from ex Situ Syntheses.* The PXRD data of the bulk reaction mixture at pH_i = 4.03 (Figure 1 in the SI) indicate compound **1**, uranium oxide hydrate (PDF 16-0207), as well as unidentified phases as components of the bulk reaction product. The originally reported synthesis of **1** did not include any impurities,[38] yet this can likely be attributed to the differences in our synthetic conditions. Figure 2 in the SI displays compounds **1**–**3** as end products of the bulk reaction mixture at pH_i = 7.95. Similarly, at pH_i = 9.00, all three compounds are present in the bulk sample (Figure 3 in the SI).

End Products from in Situ Raman Studies. Reaction Mixture at pH = 4.00. Figure 4 in the SI indicates that compound **1** and uranium oxide hydrate (PDF 16-0207) are both present within the bulk reaction product from pH = 4.00 studies. This is consistent with the PXRD data of the

dx.doi.org/10.1021/ic401143g | Inorg. Chem. 2013, 52, 9487–9495

hydrothermal ex situ reaction. Compounds **1** and **2** are found as end products of pH = 7.90 reaction studies (Figure 5 in the SI). These PXRD data, however, do not indicate the presence of **3** in the bulk product. As a minor phase, the absence of **3** is not entirely unanticipated. Moreover, upon cooling of these in situ reactions, compound **1** was identified as the sole phase in the reaction mixture. Powder data of pH = 9.00 reactions reveal the formation of compounds **1** and **2** (Figure 6 in the SI) as well as an assortment of unidentified phases.

CONCLUSION

In a general sense, we have been able to promote monomeric building unit evolution to dimeric secondary building units under the influence of pH and time. A previously reported uranyl-4,4′-BpDC material, in addition to two new uranium compounds, was synthesized hydrothermally and presents a range of structural topologies including the occurrence of a uranium(VI) CCI. These compounds (**1**−**3**) exhibited typical uranyl fluorescence and also generated characteristic Raman signatures.

The ex situ Raman spectra revealed peaks unique to single crystals of compounds **1**−**3** and, in turn, were used to monitor the formation of the title compounds within a hydrothermal in situ Raman investigation. The in situ Raman spectra at acidic conditions (pH_i = 4.00) were arguably the least complex and suggested the formation of compound **1**. At pH_i = 7.90, the in situ Raman spectra indicated the presence of compounds **1** and **3**. The most basic pH environment (9.00) created complex spectra from which none of the title compounds could be accurately detected.

In addition to Raman spectroscopy, PXRD data were utilized to identify components of the bulk reaction material. The PXRD data collected from the hydrothermal syntheses for **1**−**3** (which yielded single crystals for ex situ Raman spectra) displayed compounds **1**−**3** as end products of their corresponding synthetic conditions. The PXRD data collected from the end products of the in situ Raman reaction at pH_i = 4.00 indicated the presence of compound **1** along with uranium oxide hydrate. At a more basic pH_i (7.90), the resulting powder data suggested compounds **1** and **2** as components of the bulk end product. Similarly, in the most basic environment (pH_i = 9.00), the end products displayed both **1** and **2** along with a variety of unidentified phases. The phases identified using Raman spectroscopy and PXRD data contain disparities due to differences in experimental parameters and indeed sampling environments.

Hydrothermal in situ Raman spectroscopy has been used previously in monitoring the formation of crystalline reaction products,[62−64] single-crystal phase transitions,[65] and the kinetics and mechanisms of organic species[66,67] and characterizing the surfaces of microporous materials.[68] For our studies, it is evident that hydrothermal in situ Raman spectroscopy is an important analytical tool yet should be used in combination with other methods such as ex situ Raman and PXRD. With the addition of hydrothermal in situ Raman, we can probe further into the fundamentals of hydrothermal uranium(VI) chemistry in both the solid and solution states. Owing to the discrepancies between ex and in situ Raman methods, a cautious and informed interpretation of data should be stressed. As such, this hydrothermal uranyl system may ultimately be a candidate for in situ X-ray diffraction studies, an approach proven to be useful under similar conditions.[37,62,63,69,70]

ASSOCIATED CONTENT

Supporting Information

Hydrothermal synthesis table, PXRD patterns, additional in situ Raman spectra, bulk fluorescence spectra, bond-valence summations, table of calculated and observed Raman peaks, ORTEP figures of compounds **2** and **3**, and X-ray crystallographic data in CIF format for compounds **2** and **3** only. This material is available free of charge via the Internet at http://pubs.acs.org. CIFS have also been deposited at the Cambridge Crystallographic Database Centre and may be obtained from http://www.ccdc.cam.ac.uk by citing reference codes 937477 and 937478 for compounds **2** and **3**, respectively.

AUTHOR INFORMATION

Corresponding Author

*E-mail: cahill@gwu.edu. Phone: (202) 994-6959.

Notes

The authors declare no competing financial interest.

ACKNOWLEDGMENTS

This work supported by the Office of Basic Energy Sciences of the U.S. Department of Energy as part of the Materials Science of Actinides Energy Frontier Research Center (Grant DE-SC0001089). The authors also thank Shauo Wang (University of Notre Dame) for collecting the fluorescence data.

REFERENCES

(1) Thuéry, P. *Cryst. Growth Des.* **2011**, *11* (6), 2606−2620.
(2) Mihalcea, I.; Henry, N.; Volkringer, C.; Loiseau, T. *Cryst. Growth Des.* **2012**, *12* (1), 526−535.
(3) Volkringer, C.; Henry, N.; Grandjean, S.; Loiseau, T. *J. Am. Chem. Soc.* **2012**, *134* (2), 1275−1283.
(4) Thuery, P. *CrystEngComm* **2009**, *11* (2), 232−234.
(5) Thuery, P. *Inorg. Chem. Commun.* **2009**, *12*, 800−803.
(6) Thuery, P. *Inorg. Chem. Commun.* **2008**, *11*, 616−620.
(7) Leciejewicz, J.; Alcock, N.; Kemp, T. J. Carboxylato complexes of the uranyl ion: Effects of ligand size and coordination geometry upon molecular and crystal structure. *Coordination Chemistry*; Springer: Berlin, 1995; Vol. *82*, pp 43−84.
(8) Wang, K. X.; Chen, J. S. *Acc. Chem. Res.* **2011**, *44* (7), 531−540.
(9) Andrews, M. B.; Cahill, C. L. *Chem. Rev.* **2012**, *113* (2), 1121−1136.
(10) Allendorf, M. D.; Schwartzberg, A.; Stavila, V.; Talin, A. A. *Chem.—Eur. J.* **2011**, *17* (41), 11372−11388.
(11) Meek, S. T.; Greathouse, J. A.; Allendorf, M. D. *Adv. Mater.* **2011**, *23* (2), 249−267.
(12) Morris, W.; Doonan, C. J.; Yaghi, O. M. *Inorg. Chem.* **2011**, *50* (15), 6853−6855.
(13) Farha, O. K.; Hupp, J. T. *Acc. Chem. Res.* **2010**, *43* (8), 1166−1175.
(14) Burns, P. C. *Can. Mineral.* **2005**, *43* (6), 1839−1894.
(15) Rowland, C. E.; Cahill, C. L. *Inorg. Chem.* **2010**, *49* (19), 8668−8673.
(16) Kerr, A. T.; Cahill, C. L. *Cryst. Growth Des.* **2011**, *11* (12), 5634−5641.
(17) Lhoste, J.; Henry, N.; Roussel, P.; Loiseau, T.; Abraham, F. *Dalton Trans.* **2011**, *40* (11), 2422−2424.
(18) Morrison, J. M.; Moore-Shay, L. J.; Burns, P. C. *Inorg. Chem.* **2011**, *50* (6), 2272−2277.
(19) Sullens, T. A.; Jensen, R. A.; Shvareva, T. Y.; Albrecht-Schmitt, T. E. *J. Am. Chem. Soc.* **2004**, *126*, 2676−2677.
(20) Sullivan, J. C.; Hindman, J. C.; Zielen, A. J. *J. Am. Chem. Soc.* **1961**, *83* (16), 3373−3378.
(21) Krot, N. N.; Grigoriev, M. S. *Russ. Chem. Rev.* **2004**, *73* (1), 89−100.

(22) Albrecht-Schmitt, T. E.; Almond, P. M.; Sykora, R. E. *Inorg. Chem.* **2003**, *42* (12), 3788−3795.
(23) Mougel, V.; Horeglad, P.; Nocton, G.; Pécaut, J.; Mazzanti, M. *Angew. Chem., Int. Ed.* **2009**, *48* (45), 8477−8480.
(24) Sarsfield, M. J.; Helliwell, M. *J. Am. Chem. Soc.* **2004**, *126* (4), 1036−1037.
(25) Wilkerson, M. P.; Burns, C. J.; Dewey, H. J.; Martin, J. M.; Morris, D. E.; Paine, R. T.; Scott, B. L. *Inorg. Chem.* **2000**, *39* (23), 5277−5285.
(26) Clark, D. L.; Conradson, S. D.; Donohoe, R. J.; Keogh, D. W.; Morris, D. E.; Palmer, P. D.; Rogers, R. D.; Tait, C. D. *Inorg. Chem.* **1999**, *38* (7), 1456−1466.
(27) Guillaume, B.; Hobart, D. E.; Bourges, J. Y. *J. Inorg. Nucl. Chem.* **1981**, *43* (12), 3295−3299.
(28) Madic, C.; Guillaume, B.; Morisseau, J. C.; Moulin, J. P. *J. Inorg. Nucl. Chem.* **1979**, *41* (7), 1027−1031.
(29) Rowland, C. E.; Cahill, C. L. *Inorg. Chem.* **2010**, *49* (14), 6716−6724.
(30) Quilès, F.; Burneau, A. *Vib. Spectrosc.* **1998**, *18* (1), 61−75.
(31) Bailey, E. H.; Mosselmans, J. F. W.; Schofield, P. F. *Chem. Geol.* **2005**, *216* (1−2), 1−16.
(32) Zanonato, P.; Di Bernardo, P.; Bismondo, A.; Liu, G.; Chen, X.; Rao, L. *J. Am. Chem. Soc.* **2004**, *126* (17), 5515−5522.
(33) Redmond, M. P.; Cornet, S. M.; Woodall, S. D.; Whittaker, D.; Collison, D.; Helliwell, M.; Natrajan, L. S. *Dalton Trans.* **2011**, *40* (15), 3914−3926.
(34) Graves, P. R. *Appl. Spectrosc.* **1990**, *44* (10), 1665−1667.
(35) Ravindran, T. R.; Arora, A. K. *J. Raman Spectrosc.* **2011**, *42* (5), 885−887.
(36) He, H.; Shoesmith, D. *Phys. Chem. Chem. Phys.* **2010**, *12* (28), 8109−8118.
(37) O'Hare, D.; Evans, J. S. O.; Francis, R. J.; Shiv Halasyamani, P.; Norby, P.; Hanson, J. *Microporous Mesoporous Mater.* **1998**, *21* (4−6), 253−262.
(38) Mihalcea, I.; Henry, N.; Bousquet, T.; Volkringer, C.; Loiseau, T. *Cryst. Growth Des.* **2012**, *12* (9), 4641−4648.
(39) *APEX2*, version 3.0; Bruker Analytical X-ray Systems: Madison, WI, 2008.
(40) Sheldrick, G. *SADABS, Siemens Area Detector ABSorption Correction Program*; Universität Göttingen: Göttingen, Germany, 2008.
(41) Sheldrick, G. M. *Acta Crystallogr., Sect. A* **2008**, *64* (1), 112−122.
(42) Farrugia, L. J. *J. Appl. Crystallogr.* **1999**, *32* (4), 837−838.
(43) *JADE*, version 6.1; Materials Data Inc.: Livermore, CA, 2003.
(44) Burns, P. C.; Ewing, R. C.; Hawthorne, F. C. *Can. Mineral.* **1997**, *35* (6), 1551−1570.
(45) Brown, I. D.; Altermatt, D. *Acta Crystallogr., Sect. B* **1985**, *41* (4), 244−247.
(46) Jones, L. *J. Chem. Phys.* **1953**, *21* (3), 542.
(47) McKee, M. L.; Swart, M. *Inorg. Chem.* **2005**, *44* (20), 6975−6982.
(48) Severance, R. C.; Smith, M. D.; zur Loye, H.-C. *Inorg. Chem.* **2011**, *50* (17), 7931−7933.
(49) Mihalcea, I.; Henry, N.; Clavier, N.; Dacheux, N.; Loiseau, T. *Inorg. Chem.* **2011**, *50* (13), 6243−6249.
(50) Jones, L. H. *Spectrochim. Acta* **1959**, *15* (0), 409−411.
(51) Frost, R. L.; Čejka, J.; Weier, M. L. *J. Raman Spectrosc.* **2007**, *38* (4), 460−466.
(52) Frost, R. L.; Carmody, O.; Erickson, K. L.; Weier, M. L.; Henry, D. O.; Čejka, J. *J. Mol. Struct.* **2005**, *733* (1−3), 203−210.
(53) Bartlett, J. R.; Cooney, R. P. *J. Mol. Struct.* **1989**, *193* (0), 295−300.
(54) McGrail, B. T.; Jouffret, L. J.; Villa, E. M.; Burns, P. C. *MRS Online Proc. Library* **2012**, 1444.
(55) Toth, L. M.; Begun, G. M. *J. Phys. Chem.* **1981**, *85* (5), 547−549.
(56) Vallet, V.; Szabo, Z.; Grenthe, I. *Dalton Trans.* **2004**, *22*, 3799−3807.
(57) Tsushima, S.; Reich, T. *Chem. Phys. Lett.* **2001**, *347* (1−3), 127−132.
(58) Bell, J. T.; Biggers, R. E. *J. Mol. Spectrosc.* **1967**, *22* (1−4), 262−271.
(59) Canizarès, A.; Guimbretière, G.; Tobon, Y. A.; Raimboux, N.; Omnée, R.; Perdicakis, M.; Muzeau, B.; Leoni, E.; Alam, M. S.; Mendes, E.; Simon, D.; Matzen, G.; Corbel, C.; Barthe, M. F.; Simon, P. *J. Raman Spectrosc.* **2012**.
(60) Nguyen-Trung, C.; Palmer, D. A.; Begun, G. M.; Peiffert, C.; Mesmer, R. E. *J. Solution Chem.* **2000**, *29* (2), 101−129.
(61) Quilès, F.; Nguyen-Trung, C.; Carteret, C. d.; Humbert, B. *Inorg. Chem.* **2011**, *50* (7), 2811−2823.
(62) Pienack, N.; Bensch, W. *Angew. Chem., Int. Ed.* **2011**, *50* (9), 2014−2034.
(63) Cheetham, A. K.; Mellot, C. F. *Chem. Mater.* **1997**, *9* (11), 2269−2279.
(64) Beale, A. M.; O'Brien, M. G.; Kasunič, M.; Golobič, A.; Sanchez-Sanchez, M.; Lobo, A. J. W.; Lewis, D. W.; Wragg, D. S.; Nikitenko, S.; Bras, W.; Weckhuysen, B. M. *J. Phys. Chem. C* **2011**, *115* (14), 6331−6340.
(65) Clavier, N.; Hingant, N.; Rivenet, M.; Obbade, S. d.; Dacheux, N.; Barré, N.; Abraham, F. *Inorg. Chem.* **2010**, *49* (4), 1921−1931.
(66) Bell, W. C.; Booksh, K. S.; Myrick, M. L. *Anal. Chem.* **1998**, *70* (2), 332−339.
(67) Belsky, A. J.; Maiella, P. G.; Brill, T. B. *J. Phys. Chem. A* **1999**, *103* (21), 4253−4260.
(68) Fan, F.; Feng, Z.; Li, C. *Acc. Chem. Res.* **2009**, *43* (3), 378−387.
(69) Francis, R. J.; Price, S. J.; Evans, J. S. O.; O'Brie, S.; O'Hare, D.; Clark, S. M. *Chem. Mater.* **1996**, *8* (8), 2102−2108.
(70) Hausdorf, S.; Baitalow, F.; Seidel, J.; Mertens, F. O. R. L. *J. Phys. Chem. A* **2007**, *111* (20), 4259−4266.